Eur. Phys. J. D **14**, 71–76 (2001)

THE EUROPEAN PHYSICAL JOURNAL D

EDP Sciences

Structure determination of mixed clusters by surface scattering

E. Fort[a], H. Vach[b], M. Châtelet, A. De Martino, and F. Pradère

Laboratoire de Physique des Interfaces et des Couches Minces, CNRS, École Polytechnique, 91128 Palaiseau Cedex, France

Received 4 October 2000

Abstract. In this paper, we investigate the global structure of mixed clusters created by coexpansion. To determine the relative dopant sites within the mixed clusters, we take advantage of the strong dependence of the cluster/surface collision dynamics on the incident mixed cluster structure. Using both experiments and molecular dynamic simulations, we show that the coexpansion process leads to the most stable cluster structure for $Ar_{\langle 880\rangle}Kr_{\langle 120\rangle}$ clusters. This structure corresponds to an annealed structure and can be characterized as a nearly homogeneous mixture throughout the cluster with a thin argon coating.

PACS. 36.40.-c Atomic and molecular clusters – 34.30.+h Intramolecular energy transfer; intramolecular dynamics; dynamics of van der Waals molecules

1 Introduction

During the last two decades several experimental studies have been reported dealing with mixed van der Waals (vdW) clusters. Two techniques are commonly used to produce such mixed clusters: the *pick-up* technique invented by the Scoles group in Princeton [1] and the *coexpansion* technique. In the *pick-up* technique, pure A_n clusters consisting of n atoms of species A formed in a free jet expansion pick-up some dopant atoms of species B when passing through a buffer gas or when crossing another uncondensed beam. The *coexpansion* technique consists in expanding a gaseous mixture of two species A et B to directly produce mixed A_nB_m clusters. Because the *pick-up* technique is limited to relatively low concentrations of dopant species and large initial pure A_n clusters to avoid high beam attenuation and large velocity distribution when interacting with the buffer gas, coexpansion is preferred, or even necessary, in many experiments involving mixed clusters.

Though widely used, the process of coexpansion itself is still far from being fully understood. The modelisation is rather complex because of the many phenomena involved in both, the expansion itself (relaxation of the different degrees of freedom, focusing effect, etc.) and the binary nucleation process (number and composition of the nuclei, energy exchange between clusters and uncondensed gas). The very presence of large binary clusters resulting from coexpansion for a given gas mixture is still not trivial to forecast.

In this paper, we investigate the global cluster structure, *i.e.* the average distribution of dopant sites within a mixed cluster, for large binary clusters produced by coexpansion; we determine the relative dopant sites inside the binary cluster. This issue is of importance in the comprehension of the coexpansion process since the cluster structure is directly coupled with the cluster nucleation and growing process, and its interaction with the surrounding gas.

In addition, understanding binary cluster structure yields precious information concerning the related phenomena such as species mixing, segregation and coexisting phases. Only few theoretical studies have addressed these questions [2–6] and even fewer experimental investigations have been performed dealing with mixed clusters containing more than a few atoms of each species [7–9].

To investigate the global mixed cluster structure obtained by coexpansion, we present an original technique based on the surface collision dynamics. When binary vdW clusters at thermal incident velocities are scattered from a surface, they are known to exhibit a Leidenfrost-like dynamics [9–11]; *i.e.* the binary clusters glide along the surface evaporating thermalized guest and host atoms to evacuate the collision energy. Large fragments, scattered at grazing angles, may survive for sufficiently "soft" collisions [11].

In a recent paper [12], we have experimentally measured different evaporation temperatures for the two species during the surface collision of mixed $Ar_{\langle 880\rangle}Kr_{\langle 120\rangle}$ clusters obtained by krypton pick-up: 280 and 190 K for krypton and argon, respectively. The difference between these two temperatures was tentatively attributed to the crucial role played by the incident cluster structure. This hypothesis has been validated using molecular dynamics (MD) simulations by comparing the collision dynamics of two different initial cluster structures [13]. The first structure, called *belt* structure, is obtained by simulating the pick-up process and, consequently, is expected to be

[a] *Present address*: Laboratoire de Minéralogie-Cristallographie, Universités Paris VI et VII, Paris.
e-mail: `fort@lmcp.jussieu.fr`
[b] e-mail: `vach@leornado.polytechnique.fr`

very similar to the experimental cluster structure: krypton atoms are confined close to the cluster surface layers due to their limited intra-cluster diffusion. In the second structure, referred to as the *core* structure, krypton atoms form a core in the very cluster center.

The *belt* structure, on one hand, gives evaporation temperature values similar to the experimental ones; *i.e.* an evaporating temperature for krypton that is 90 K hotter than that for argon. The *core* structure, on the other hand, gives a colder evaporation temperature for krypton than for argon, 150 *versus* 190 K, demonstrating the high sensibility of the collision dynamics toward the incident cluster structure. In the present paper, we take advantage of this dependence to obtain the global structure of mixed $Ar_{\langle 880\rangle}Kr_{\langle 120\rangle}$ clusters produced by coexpansion.

This paper is structured as follows: the following section is devoted to the setup and the data analysis description. Section 3 gives the model and the calculational details for the MD simulations. Our results are presented and discussed in Section 4.

2 Experimental setup and data analysis

Our experimental setup has been described in detail previously [14]. In this section, we summarize the essential parts that are of interest for the new results presented in this paper. We use a supersonic Campargue-type beam generator with a conical nozzle (with 0.12 mm diameter and 5° half-angle). The beam passes through three differentially pumped chambers before entering an Ultra-High Vacuum (UHV) chamber. We can introduce a buffer gas in the third chamber either directly to permit average cluster size determination [15] or through a small pipe positioned in the beam path for the pick-up process [11].

Beam diagnostics are performed using a rotatable Quadrupole Mass Spectrometer (QMS) in the UHV chamber. The QMS mass range extends to 200 amu and can consequently only detect relatively small particles. When larger fragments enter the ionization head of the QMS, they are fragmented into small particles before being detected [14,16]. The QMS rotates about the center of the UHV chamber where a surface sample can be placed to intercept the beam. The beam is modulated by a chopper in the third vacuum chamber to allow lock-in detection of the flux and time-of-flight measurements.

Mixed $Ar_{\langle 880\rangle}Kr_{\langle 120\rangle}$ clusters are obtained by coexpansion of a gas mixture with 1.5% of krypton in argon. The relative composition of the mixed clusters is obtained from QMS flux measurements in the cluster beam at the species mass settings using the appropriate sensitivity corrections.

The size of the clusters is determined by the profile broadening technique [15]. When passing through a buffer gas the beam profile broadens. From the measurement of this broadening as a function of the buffer gas pressure, it is possible to deduce the average cluster size in the incident beam. The uncertainty of our size measurement technique is within 50% of the cluster size for both pure and mixed clusters.

In the present paper, we used a Highly Oriented Pyrolytic Graphite (HOPG) surface at a temperature of 550 K and the incidence angle of the impinging $Ar_{\langle 880\rangle}Kr_{\langle 120\rangle}$ clusters was set to 30°. Their incident velocity was (470 ± 20) m/s.

As mentioned in the introduction, for thermal incident kinetic energies, the dynamics of the vdW cluster collision with a surface can be understood as follows: the impinging clusters undergo an inelastic collision in which they glide on the surface, hovering on a gaseous "cushion" while evaporating thermalized small particles. Apart from this main *evaporation* channel, two other scattering channels can be detected: the *diffusion* channel composed of cluster atoms that undergo a trapping/desorption process and a *grazing* channel of slow and large fragments that survive the collision [11].

To describe the evaporation channel, we developed a *thermokinetic* (TK) model [16] in which particles are evaporated thermally at a local temperature $T_{\rm loc}$ from a cluster moving with the velocity $c_{\rm f}v_{\parallel}$ on the surface where $c_{\rm f}$ is the conservation coefficient of the incident velocity component parallel to the surface $v_{\parallel}$. These two parameters, $T_{\rm loc}$ and $c_{\rm f}$, are obtained by fitting the angular distributions of flux (AFD) and of time-of-flight (ADTOF) for the scattered particles of the evaporation component. This model describes very well the experimental results for a large range of experimental conditions for the surface scattering of both pure and mixed clusters in the evaporation regime [11,16].

3 Model and calculational details

Most of the calculational details have been published previously [4,17]. Here, we just like to remind the reader that we use the methods of molecular dynamics simulations to simulate the cluster surface scattering; *i.e.*, we integrate the Newtonian equations of motion for all interacting particles yielding their phase space trajectories. In the present paper, we describe the intracluster interactions between all atoms by additive, pairwise 6-12 Lennard-Jones (LJ) potentials. For the Ar–Ar interaction, we use 3.405 Å and 119.8 K, and for the Kr–Kr interaction, 3.591 Å and 172.7 K for the interatomic distance σ and the potential well depth ϵ, respectively. For the Ar–Kr interaction parameters the following combining rules have been used $\sigma_{\rm Ar-Kr} = (\sigma_{\rm Ar-Ar} + \sigma_{\rm Kr-Kr})/2$ and $\epsilon_{\rm Ar-Kr} = \sqrt{\epsilon_{\rm Ar-Ar}\epsilon_{\rm Kr-Kr}}$ [6].

The cluster structure we use in the present MD simulations has been obtained by high-pressure pick-up of krypton on a neat argon cluster [4]. The initial argon clusters undergo a phase transition to the liquid phase during their flight through the pick-up zone because evaporation alone cannot evacuate all the heat resulting from the collisions with the buffer gas. The initial FCC-structure is completely lost in this process and krypton atoms penetrate deeply into the argon host cluster. After the pick-up zone, the mixed $Ar_{880}Kr_{120}$ clusters are then allowed to cool down by flying freely for 228 ns. They start recrystallizing into a FCC-structure at about 21 ns after the

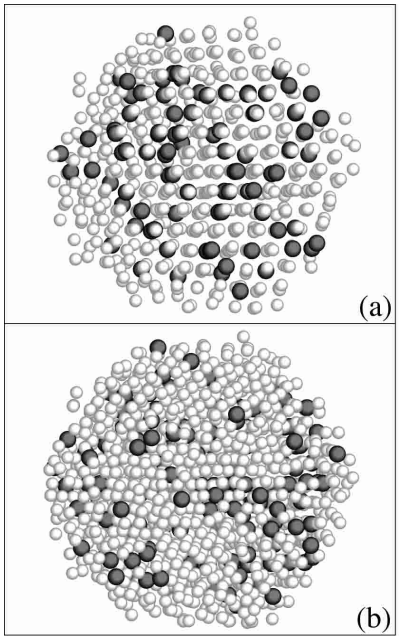

Fig. 1. Snapshots of an $Ar_{880}Kr_{120}$ cluster with an *annealed* structure. This structure is obtained by MD simulations after the subsequent cooling down from a high pressure pick-up that induced a solid-liquid phase transition for the entire cluster in the pick-up zone: (a) cut through its center and (b) entire cluster.

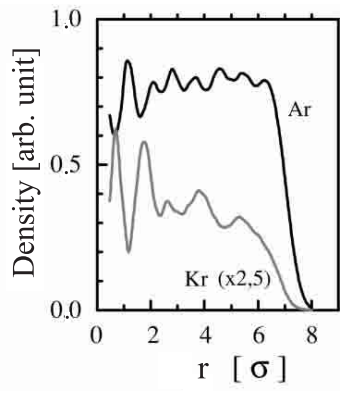

Fig. 2. Radial density function for both Ar and Kr atoms for an $Ar_{880}Kr_{120}$ cluster obtained after high pressure pick-up.

pick-up process. The krypton atoms find their final positions in substitution position in the argon lattice. Figure 1 presents two snapshots of the mixed cluster after it has cooled down: (a) is a cut through the center of the cluster and (b) is a view of the entire cluster. Figure 2 gives the radial density function of this cluster. The krypton dopants appear homogeneously distributed throughout the entire cluster with a somewhat higher density in the center. Note that this density profile is similar to the one obtained for larger clusters with the same dopant fraction in the same conditions [4].

It is important to note that the high-pressure pick-up process described above is far from the usual experimental conditions: under our normal experimental pick-up conditions, the buffer gas pressure is typically about 5 000 times lower than for the high pressure pick-up considered here. Hence, the structure obtained by this high pressure method is called in the following the *annealed* structure referring to the solid-liquid phase transition undergone temporarily by the entire cluster.

A model for the surface scattering simulations has been described in detail in reference [17]. Basically, it takes into account the quasi-trapping mechanism that has been demonstrated to best describe the interaction of argon clusters with a graphite surface. The trapping probability under the presently employed experimental conditions is found to be around 50% [18]. To consider such an interaction dynamics in the framework of our present MD simulations, we assume that half of the randomly chosen surface touching cluster atoms are scattered off a perfectly flat and hard surface and that the other half undergoes a quasi-trapping process for which the surface residence time is defined in terms of a first order desorption kinetics:

$$\tau = \frac{h_{\mathrm{P}}}{k_{\mathrm{B}} T_{\mathrm{S}}} \exp\left[\frac{E_{\mathrm{S}}}{k_{\mathrm{B}} T_{\mathrm{S}}}\right] \tag{1}$$

where h_{P} is Planck's constant, k_{B} is Boltzmann's constant, T_{S} is the surface temperature, and E_{S} is the binding energy of a given cluster atom to the graphite surface. After this residence time, quasi-trapped atoms are desorbed thermally accommodated to the surface temperature in randomly chosen directions. In this manner, the cluster-surface collision is simulated in the same way as in reference [13] in order to facilitate the comparison. We like to point out that this very simple quasitrapping model gives excellent agreement with *all* our recent experimental results for the scattering of large argon clusters from a graphite surface [17]. We have performed 48 independent trajectories to reduce the statistical noise varying the initial cluster velocity between 450 and 490 m/s and choosing random orientations for the incident clusters.

4 Results and discussions

Figure 3 presents the measured angular flux distribution (AFD) of the scattered argon and krypton particles for mixed $Ar_{\langle 880\rangle}Kr_{\langle 120\rangle}$ clusters obtained by coexpansion and impinging on a HOPG surface with a velocity of 470 m/s and an incidence angle of 30°. These conditions lead typically to a cluster/surface interaction dynamics in the thermal evaporation regime. We observe, for both species, a narrow peak at grazing scattering angles of about 78° indicating the survival of large cluster fragments. The relative flux proportion associated with this peak is larger for krypton than for argon. These peaks are asymmetric and broad shoulders are clearly visible for both components for detection angles between 25° and 60°.

The angular distributions of the most probable time-of-flight between surface and detector (ADTOF) are represented in Figure 4 for both species. The main results are

Table 1. Evaporation temperatures obtained experimentally and by MD simulations for argon and krypton resulting from the surface collision of mixed $Ar_{\langle 880\rangle}Kr_{\langle 120\rangle}$ clusters. Temperatures are given in Kelvin.

	MD simulations			experiments	
structure	core	annealed	belt	pick-up	coexpansion
$T_{\rm loc}$(Kr)	150 ± 30	227 ± 35	280 ± 30	280 ± 30	237 ± 30
$T_{\rm loc}$(Ar)	190 ± 10	187 ± 7	190 ± 10	190 ± 15	182 ± 15
$\Delta T_{\rm loc}$	-40	$+40$	$+90$	$+90$	$+55$

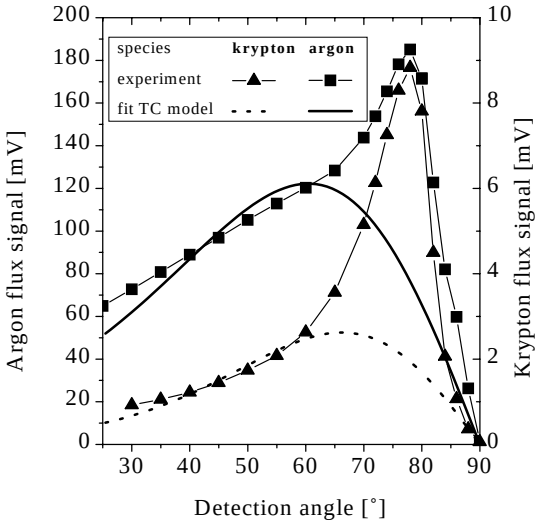

Fig. 3. Experimental angular flux distributions (AFD) for the scattered atoms after the surface collision of $Ar_{\langle 880\rangle}Kr_{\langle 120\rangle}$ clusters produced by coexpansion. The fit obtained with the thermokinetic model (TK) has also been presented.

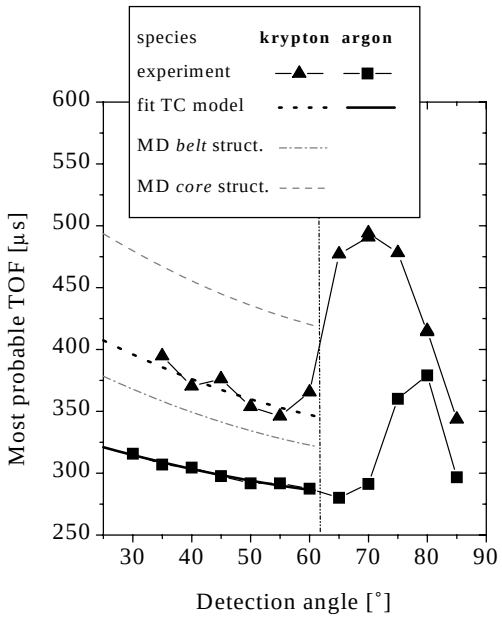

Fig. 4. Experimental angular distributions of the most probable time-of-flight (ADTOF) for the scattered atoms after the surface collision of $Ar_{\langle 880\rangle}Kr_{\langle 120\rangle}$ clusters produced by coexpansion. The fit obtained with the thermokinetic model (TK) has also been presented together with TK fits to the simulated flight times for krypton obtained from incident *belt* and *core* structures.

interpreted as follows:

- in the detection range of 30° to 60°, the *evaporation* channel consisting of small fragments evaporating thermalized from the gliding parent cluster is dominant. We use the *thermokinetic* model to fit the AFD and ADTOF curves in this scattering angle range. These fits presented in Figures 3 and 4 for both species use only two parameters, the conservation coefficient $c_{\rm f}$ of the incident tangential velocity component and the average evaporation temperature $T_{\rm loc}$ for each species. We obtain 182 and 237 K for this temperature for argon and krypton, respectively (see Tab. 1). The coefficient $c_{\rm f}$ is 0.9 for both species;
- like for the AFD, the ADTOF curves clearly show a second type of scattering channel: at grazing angles the scattered particles are slow compared with the ones detected between 30° and 60°. In this range, the velocity of the particles increases slightly with increasing scattering angle. The peaks in the AFD curves associated with slow particles in the ADTOF are attributed to large fragments surviving the collision. We find that the proportion of krypton in these large fragments is more important than in the incident cluster. This enrichment has been observed previously for mixed $Ar_{\langle 880\rangle}Kr_{\langle 120\rangle}$ clusters produced by pick-up colliding on a graphite surface [11]. It can be attributed to the higher binding energy of krypton atoms compared to argon atoms that, consequently, have a higher probability to evaporate thermally during the collision process than the krypton atoms;
- finally, we like to mention that for smaller and negative scattering angles, the *trapping-desorption* channel due to particles getting temporarily trapped on the surface [18], is no longer negligible. This channel actually limits the applicability of the TC model to scattering angles that are larger than 25°.

We now use the surface scattering results to deduce the initial structure of the mixed clusters produced by coexpansion. In Table 1, we have gathered the local temperatures, for both species, obtained experimentally for the same type of mixed clusters produced either by coexpansion or by pick-up (see Ref. [12]). Besides, we also present the evaporation temperatures $T_{\rm loc}$ obtained by MD simulations for three different initial cluster structures: the

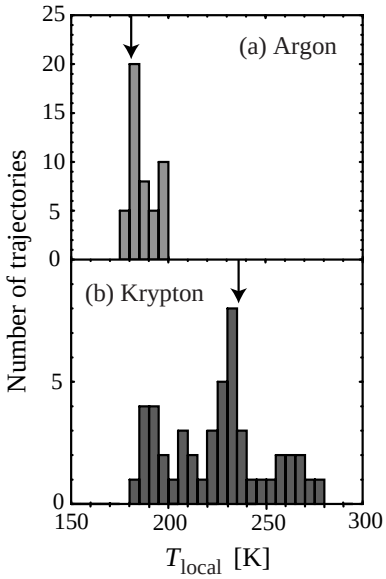

Fig. 5. Evaporation temperature histograms for scattered argon and krypton atoms after the surface collision of an $Ar_{880}Kr_{120}$ cluster with an *annealed* structure. 48 independent trajectories have been simulated. The arrows indicate the experimental values obtained for clusters produced by coexpansion.

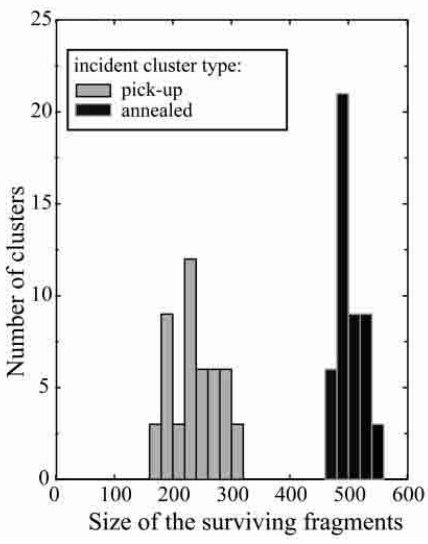

Fig. 6. Size histograms of the surviving clusters resulting from the surface scattering of $Ar_{880}Kr_{120}$ clusters created either by coexpansion (annealed structure) or by low pressure pick-up (belt structure). 48 independent trajectories have been simulated.

belt and the *core* structures (see Ref. [13]) and the *annealed* structure (described in Sect. 3).

The evaporation temperatures obtained experimentally for mixed clusters produced by coexpansion and pick-up are quite similar for argon, but differ significantly for krypton: the dopant evaporation temperature is 43 K lower for the coexpansion clusters than for the ones created by pick-up. The evaporation temperature obtained by MD simulations for argon is always the same, independent of the initial cluster structure and quantitatively very similar to the experimental one. As we showed in reference [13], the position of the dopants in the cluster plays a crucial role in the evaporation process: the krypton evaporation temperature varies by 130 K between the two extremes of *core* and *belt* structure.

Furthermore, the results presented in Table 1 confirm that the *belt* structure, generated by simulating a pick-up process under quasi-experimental conditions, is indeed identical to the one obtained experimentally for clusters produced by this technique. In the same way, it is also possible to deduce the structure of mixed clusters produced by coexpansion. Indeed, from Table 1, it is clear that the krypton evaporation temperature obtained experimentally for clusters produced by coexpansion is only consistent with the simulated *annealed* cluster structure presented in Figures 1 and 2. Figure 5 presents the species resolved evaporation temperature histogram for the annealed structure. The local temperature distribution of the evaporated argon atoms is very narrow (FWHM 7 K) and centered at 187 K whereas the krypton temperature turns out to be 40 K hotter and broader (FWHM 35 K). The experimental results have also been presented for comparison (see arrows). Simulated and experimental values are in good agreement.

We also like to point out that the incident cluster structure does not only determine the dopant evaporation temperature in a very crucial way, but also the angular flux distributions resulting from the surface scattering. The AFD curves obtained from clusters produced by coexpansion (*cf.* Fig. 3) and by pick-up (*cf.* Fig. 1 in Ref. [12]) present a striking difference: in the former case, a peak is clearly visible at grazing angles for both species while in the latter, such peaks are absent. In both cases, large fragments *do* survive the collision, as can be deduced from the low velocity peaks in the ADTOF. Nevertheless, the size of these surviving fragments differs dramatically: while for clusters produced by pick-up, the surviving fragments are too small to be detected in the AFD because of the presence of the dominant evaporation channel, clusters produced by coexpansion yield much larger fragments clearly visible in the AFD.

Our MD simulations lead to the same results as can be seen in the histograms of the surviving fragment sizes presented in Figure 6 for both types of incident cluster structures: after the surface scattering, $Ar_{880}Kr_{120}$ clusters created by pick-up give surviving fragments of about 200 atoms while the same size clusters produced by coexpansion yield 500 atom fragments.

The simulated *annealed* cluster structure obtained by high pressure pick-up of krypton on pure argon cluster is very similar to the one described by Clarke *et al.* [3]. They studied the equilibrium structural properties of binary LJ clusters by MD simulations, in particular $Ar_{55}Kr_{55}$ clusters. They showed a "considerable mixing between the two species" with a higher concentration of krypton at the center and of argon at the surface. Zeng *et al.* [2]

confirmed such a structure by means of density functional theory on a $Ar_{87}Kr_{128}$ nucleus at $T = 115.77$ K. They estimated the argon molar fraction at the center to be only 0.264 and observed also an argon enrichment at the surface. High pressure pick-up thus leads to the most stable mixed cluster structure. This is not surprising since the entire cluster undergoes a phase transition to the liquid phase and is not allowed to cool down during the whole pick-up process due to the very large number of collisions with the high density buffer gas atoms.

The higher stability of the incident clusters obtained by high pressure pick-up or coexpansion results in larger surviving fragments after the surface collision compared with those created by low pressure pick-up. The average potential energy per atom is -730 K and -685 K for the *annealed* and the *belt* structure, respectively. For comparison, the simulated *core* structure in reference [13], gives surviving cluster sizes of about 300 atoms and an average potential energy per atom of -710 K. These data prove that the surviving cluster size depends very sensitively on the binding energy.

The nucleation process during the coexpansion is consequently allowing the clusters to reach the most stable configurational state. Collisions with the surrounding molecules are sufficiently numerous to keep the cluster liquid and to allow diffusion of the cluster atoms. Cluster evaporation is not sufficient to evacuate all the heat resulting from the collisions. Therefore, a relatively high cluster temperature is reached, very much like during the simulated high pressure pick-up process [4]. Hence, the relative krypton dopant site distribution for the mixed $Ar_{\langle 880\rangle}Kr_{\langle 120\rangle}$ clusters created experimentally by coexpansion should be very similar to the one shown in Figures 1 and 2 from MD simulations.

While it seems to be reasonable, it could not have been assumed from the beginning that mixed clusters produced by coexpansion reach their most stable configuration. For, experimental studies have shown that the most condensible species is the first to nucleate during the expansion process [9]. Consequently, the clusters might take temporarily a *core* structure during the early stage of the nucleation process and only the dynamical interaction between the forming nuclei and the surrounding gas allows them to reach their most stable configuration further downstream.

Finally, we would like to mention that electron diffraction studies performed, for instance, by the Orsay group [7] and our surface scattering technique give very complementary results concerning the mixed cluster structure: electron diffraction gives access to the overall crystal structure of the clusters while surface scattering probes the relative dopant sites inside the clusters.

5 Conclusion

In this paper, we investigated the structure of mixed clusters created by coexpansion. By surface scattering, we determined the relative position of krypton dopants within an argon cluster taking advantage of the strong dependence of the collision dynamics on the incident cluster structure. In our experiments, we observed that the two species in the mixed cluster evaporate at markedly different temperatures during the surface collision. Using MD simulations, we showed that this temperature difference is very sensitive to the incident cluster structure. This measured temperature difference is used to determine the structure of $Ar_{\langle 880\rangle}Kr_{\langle 120\rangle}$ mixed clusters produced by coexpansion. We give evidence that this structure is similar to the one obtained from an annealing process involving a complete solid-liquid phase transition within the entire cluster: the krypton penetrates deeply into the cluster and is distributed homogeneously throughout the whole cluster after cooling down to its final temperature. This structure, which is predicted to be the most stable configuration, gives also experimentally the largest surviving fragments after the surface interaction.

Most of the calculations were carried out at the French National Computer Center IDRIS. We would like to acknowledge the computer time that was allotted for the present study. We also thank those at the computer center of the École Polytechnique DSI who provided us very generously with CPU time on their local work stations.

References

1. T.E. Gough, M. Mengel, P. Rowntree, G. Scoles, J. Chem. Phys. **83**, 4958 (1985).
2. X.C. Zeng, D.W. Oxtoby, J. Chem. Phys. **95**, 5940 (1991).
3. A.S. Clarke, R. Kapraf, G.N. Patey, J. Chem. Phys. **101**, 2432 (1994).
4. H. Vach, J. Chem. Phys. **111**, 3536 (1999).
5. H. Vach, Phys. Rev. B **59**, 13413 (1999).
6. L. Perera, F.G. Amar, J. Chem. Phys. **93**, 4884 (1990).
7. G. Torchet, M.-F. de Feraudy, Y. Loreaux, J. Molec. Struct. **485**, 261 (1999).
8. E.J. Valente, L.S. Bartell, J. Chem. Phys. **79**, 2683 (1983).
9. E. Fort, F. Pradère, A. De Martino, M. Châtelet, H. Vach, Eur. Phys. J. D **1**, 79 (1998).
10. N. Marković, J.B.C. Pettersson, J. Chem. Phys. **100**, 3911 (1994).
11. E. Fort, A. De Martino, F. Pradère, M. Châtelet, H. Vach, J. Chem. Phys. **110**, 2579 (1998).
12. E. Fort, H. Vach, A. De Martino, M. Châtelet, F. Pradère, Eur. Phys. J. D **7**, 229 (1999).
13. H. Vach, E. Fort, A. De Martino, M. Châtelet, F. Pradère, Chem. Phys. Lett. **314**, 552 (1999).
14. F. Pradère, M. Benslimane, M. Château, M. Bierry, M. Châtelet, D. Clément, A. Guilbaud, J.-C. Jeannot, A. De Martino, H. Vach, Rev. Sc. Instrum. **65**, 161 (1994).
15. A. De Martino, M. Benslimane, M. Châtelet, C. Crozes, F. Pradère, H. Vach, Z. Phys. D **27**, 185 (1993).
16. H. Vach, A. De Martino, M. Benslimane, M. Châtelet, F. Pradère, J. Chem. Phys. **100**, 3526 (1994).
17. H. Vach, Phys. Rev. B **61**, 2310 (2000).
18. M. Benslimane, M. Châtelet, A. De Martino, F. Pradère, H. Vach, Chem. Phys. Lett. **237**, 323 (1995).